

# **SURFACE MODIFICATION OF POLY (ETHYLENE TEREPHTHALATE) (PET) FOR MULTIFUNCTIONAL PROPERTIES**

**KARAN CHANDRAKAR**



**DEPARTMENT OF TEXTILE AND FIBRE ENGINEERING  
INDIAN INSTITUTE OF TECHNOLOGY DELHI  
MAY 2025**

**© Indian Institute of Technology Delhi (IITD), New Delhi, 2025**

**SURFACE MODIFICATION OF POLY(ETHYLENE  
TEREPHTHALATE) (PET) FOR  
MULTIFUNCTIONAL PROPERTIES**

**by**

**KARAN CHANDRAKAR**

**Department of Textile and Fibre Engineering**

Submitted

in fulfillment of the requirements of the degree of

**Doctor of Philosophy**

to the



**INDIAN INSTITUTE OF TECHNOLOGY DELHI**

**May 2025**

**Dedicated to**

**My Mother (Late Smt. Rajkumari  
Chandrakar), my Bua Ji (Late Smt.  
Shakuntala Chandrakar)**

**and**

**Especially to my supervisors**

**Prof. Ashwini K. Agrawal and Prof. Manjeet  
Jassal**

## CERTIFICATE

This is to certify that the thesis titled “**Surface modification of poly(ethylene terephthalate) (PET) for multifunctional properties**” being submitted by **Mr. Karan Chandrakar** to the **Indian Institute of Technology Delhi** for the award of the degree of **Doctor of Philosophy**, is a record of bonafide research work carried out by him. He has worked under our guidance and supervision and fulfilled the requirements for the submission of the thesis, which has attained the standard required for a Ph.D. degree of this Institute.

The results contained in this thesis have not been submitted, in part or in full, to any other university or institute for the award of any degree or diploma.

**Dr. Ashwini K. Agrawal**  
Professor  
Department of Textile and Fibre  
Engineering  
Indian Institute of Technology Delhi

**Dr. Manjeet Jassal**  
Professor  
Department of Textile and Fibre  
Engineering  
Indian Institute of Technology Delhi

Date:  
New Delhi



## ACKNOWLEDGEMENTS

I express my heartfelt gratitude to all people, whose invaluable contributions played a vital role in the success of this thesis. Without their support, this journey would not have been possible. Their insightful advice and their dedicated efforts played a pivotal role in turning this endeavor into a reality.

First and foremost, I would like to express my gratitude towards Lord Krishna, for being my internal compass in this journey. Without the spiritual strength from Bhagwat Geeta, I would not have the energy and the willingness to continue to push forward in the long hours of day and night for the past several years.

I want to convey my deepest appreciation to Prof. Ashwini K. Agrawal and Prof. Manjeet Jassal from the Department of Textile and Fibre Engineering at IIT Delhi who have been my north star in this journey. They have generously offered their guidance, support, and motivation from the outset until the completion of this thesis. I will forever be grateful to them for dedicating their time for my success, fostering an excellent research atmosphere, and empowering me with the necessary tools to thrive.

I would also like to extend my gratitude to Prof. R. Alagirusamy, the current Head of the Department of Textile Technology and Fibre Engineering, as well as to the former Heads of Department, Prof. B.K Behra, Prof. Kushal Sen and Prof. Ashwini K. Agrawal for their cooperation, which facilitated the seamless completion of this research work. Furthermore, I extend my thanks to the members of my SRC (Student Research

Committee), Prof. B.S Butola, Prof. Rajiv Srivastava, and Prof. Leena Nebhani, for sharing their valuable suggestions.

I would like to acknowledge the Ministry of Human Resource Development (MHRD), Government of India, for the financial support. I would also like to thank the Department of Science and Technology (DST) for providing necessary research facilities through various research grants to the SMITA Research Lab.

I would like to express my gratitude to the department's staff, particularly Mr. Amarjit, Mr. Raj Kumar, Mr. Rajinder Khatter, Mr. Vikas Khatkar and Mr. Rohit Kumar, for their technical support and their cooperation throughout my doctoral studies.

I extend my appreciation to the members of CRF and NRF, particularly Dr. Atul Kumar Singh, Mr. Kuldeep Sharma, Ms. Kumud Arora, Mr. Rajesh Kumar, Mr. Animesh Bhowal, and Ms. Aastha Sharma, for their support in conducting various experimental studies throughout my Ph.D. work.

I am grateful to Sarojmukh Madhav Das, Pandav Kesav prabhu ji and Sandeep , I have met during this journey in ISKCON Jia-Sari BACE. They have been a constant source of support, who have stood by my side through both joyful and challenging moments. Their presence has made this journey truly unforgettable, and I will cherish the memories we shared throughout my life. Thank you for being such wonderful spiritual companions.


Also, it gives me immense joy and privilege to extend my appreciation to senior members at SMITA Research Lab, Dr. Hardeep Singh Jhinjer, Dr. Neeta Kumari, Dr. Rashmi Agrawal, Dr. Kiran Yadav, Dr. Deepika Gupta, Dr. Gurneet Kaur, Mrs. Nayana J Nair, and Ms. Kiran Rana. I deeply appreciate their willingness to share their valuable time to teach me various laboratory instruments and techniques, their knowledge, and their unwavering encouragement. I would like to express my special thanks to the members of the SMITA Research Lab and my wonderful companions, including Mr. Rajesh Kumar, Mr. Pranay Ahuja, Mr. Gopal Kumar, Mr. Jovanpreet Singh, Mr. Suraj Singh, Mr. Ankit Shankar, Mr. Maitreyi, Mr. Ram Agrawal, Mr. Akhilesh Kumar, Mr. Adarsh Partap Singh, and Mr. Jogender Rathore, for fostering a positive and supportive lab environment in which I was able to conduct my research seamlessly. They have consistently been available for discussions and readily helped whenever needed. I am also very thankful to the staff of the SMITA Research Lab, Mr. Praveen, Mr. Arvind, and Mr. Manjeet.

I am at a loss for words to express my deep appreciation to my entire family for their unwavering support throughout my entire educational journey. I want to thank my mother (late Smt Rajkumari Chandrakar), my bua ji (Late Smt. Shakuntala Chandrakar), my father (Sri Chandrashekhar Chandrakar), my wife (Mrs. Preeti Chandrakar), my loving daughter (Baby Parthivi Chandrakar) and my younger sister (Ms. Namrata Chandrakar) for their endless support and encouragement to complete this journey.

I would like to extend my heartfelt gratitude to all my well-wishers and those who have been a part of my journey, whose unwavering support and boundless encouragement have uplifted me through every challenge life has presented.

I express my sincere thanks to all those who have helped me directly or indirectly all through my research work. I will cherish each person's valuable time, contributions, and their sacrifices towards success of my goal throughout my life.

To all the individuals mentioned above and to those whose names may have been inadvertently excluded, please know that your support has been deeply valued and cherished.



Karan Chandrakar

Department of Textile and Fiber Engineering

Indian Institute of Technology Delhi

## ABSTRACT

Enhancing the functional performance of synthetic textiles, especially poly(ethylene terephthalate) (PET), is a key focus in material science and textile engineering. While PET is popular in active wear due to its durability and light weight, its hydrophobicity and flammability pose challenges for moisture management and safety. To overcome these issues, the aim of this study is to investigate surface modification of PET with advanced nanomaterials like nanodiamonds (NDs) and hydroxyapatite (HAp), aiming for multifunctional and sustainable high-performance textiles.

Nanodiamonds (NDs) have emerged as a promising class of carbon nanomaterials, used for their unique properties including low toxicity, ease of surface functionalization, and excellent biocompatibility. Traditionally, NDs are synthesized through methods, which are energy-intensive, require hazardous chemicals, and involve lengthy reaction times. Recognizing the need for more sustainable alternatives, this study investigates the synthesis of NDs via probe ultrasonication at ambient temperature and pressure, using organic salts as precursors in an aqueous medium. This method significantly reduces environmental impact and operational complexity. Characterization techniques such as FESEM, HRTEM, FTIR, Raman, and XRD revealed that ultrasonication time is a critical factor: shorter durations (30 min) yield metastable morphologies, while longer ultrasonication (1 hour) produces high-quality cubic nanodiamonds. Acid purification further sharpens the diamond Raman peak at  $1332\text{ cm}^{-1}$  and confirms the cubic crystal structure, demonstrating that this green approach can reliably produce well-defined NDs and its *in-situ* and *ex-situ* application of PET surface to achieve

multifunctionalities such as water absorbency and fire retardancy. The development enables the scalable production of nanodiamonds for advanced textile applications without compromising environmental safety.

Building upon the green synthesis of NDs, the next part of the study discusses their direct application onto PET fabrics to address the flammability and hydrophobicity of PET fabric. In this study, a novel *in-situ* approach is employed, wherein carbon nanostructures are synthesized directly on the PET surface using atmospheric pressure dielectric plasma. This approach eliminates the requirement for independent nanoparticle synthesis and later deposition, resulting in a more consistent and firmly attached nanodiamond coating on the textile fibres. FESEM and HRTEM analyses confirm the presence and morphology of the carbon nanostructures, while Raman and FTIR spectroscopy validate the formation of NDs and their chemical integration with the fabric. The functionalized PET fabrics exhibit marked improvements in flame retardancy, with LOI values up to 26-28, as well as enhanced hydrophilicity, which is crucial for comfort and moisture management in active wear. *In-situ* functionalization not only simplifies the process but also produces textiles with durable, multi-functional properties.

While treatment with NDs significantly improve flame resistance and surface hydrophilicity, further enhancements in moisture management and UV protection are desirable for high-performance active wear. To this end, hydroxyapatite (HAp), a biocompatible ceramic commonly found in bone and teeth, was explored as a surface coating for PET fabrics. In this study, HAp was synthesized via two distinct chemical precipitation methods (coded as HAp1 and HAp2) and applied *ex-situ* to PET using a

dip-pad-cure process. Both HAp coatings resulted in notable improvements in water absorbency, wicking ability, quick-drying behavior, and ultraviolet protection factor (UPF). However, fabrics treated with HAp1 demonstrate superior performance and durability, even after multiple washing cycles. Detailed characterization using FESEM, FTIR, Raman, and XPS reveals that the HAp1 process yields finer particles that interact more intimately with the PET fiber surface, leading to stronger adhesion and more robust functional properties. The successful application of HAp coatings not only addresses the hydrophobicity of PET but also introduces multifunctionality.

Recognizing the promising results of HAp coatings, the further studies were directed towards the *in-situ* synthesis of hydroxyapatite (In-HAp1 and In-HAp2) directly on PET fabrics. This approach aimed to maximize the functional benefits of HAp while ensuring long-term durability under real-world conditions. The *in-situ* dip-pad-cure method produces a uniform and continuous HAp layer, with In-HAp1 in particular yielding a nanoscale coating that adheres tightly to the fiber surface. Comprehensive evaluations using FESEM, FTIR, Raman, and XPS demonstrate that In-HAp1-treated fabrics maintain their enhanced UPF and moisture management properties even after repeated washing, outperforming In-HAp2. The improved performance is attributed to the controlled growth and finer particle size achieved in the In-HAp1 process, which facilitate stronger interactions with the PET substrate, which were higher than the previous *ex-situ* HAp coating. By leveraging the hydrophilic and UV-blocking properties of HAp, this optimized surface modification transforms PET into a truly multifunctional textile, ideally suited for sustainable, high-performance active wear. Each section of this research builds upon the previous one, starting with the development of a sustainable method for nanodiamond synthesis, moving to their direct

application for flame retardancy and hydrophilicity in PET, and then addressing further enhancements in moisture management and UV protection through bio-ceramic such as hydroxyapatite coatings. By integrating these advanced surface modifications, the research sets a foundation for the next generation of smart, multifunctional, and sustainable textiles.

## सारांश

सिंथेटिक वस्त्रों, विशेष रूप से पॉलीइथाइलीन टेरेफ्थैलेट (PET) के कार्यात्मक प्रदर्शन को बढ़ाना, सामग्री विज्ञान और वस्त्र अभियांत्रिकी में एक प्रमुख फोकस है। जबकि PET अपनी मजबूती और हल्केपन के कारण सक्रिय परिधान में लोकप्रिय है, इसकी जल-विरोधिता (हाइड्रोफोबिसिटी) और ज्वलनशीलता (फ्लेमबिलिटी) नमी प्रबंधन और सुरक्षा के लिए चुनौतियाँ प्रस्तुत करती हैं। इन समस्याओं को दूर करने के लिए, इस अध्ययन का उद्देश्य PET की सतह को उन्नत नैनोमटेरियल्स जैसे नैनोडायमंड (NDs) और हाइड्रॉक्सीएपेटाइट (HAp) से संशोधित करने की जांच करना है, ताकि बहु-कार्यात्मक और टिकाऊ उच्च-प्रदर्शन वस्त्र प्राप्त किए जा सकें।

नैनोडायमंड (NDs) कार्बन नैनोमटेरियल्स का एक उभरता हुआ वर्ग है, जिसे उनकी अद्वितीय विशेषताओं जैसे कम विषाक्तता, सतह क्रियाशीलता में आसानी और उत्कृष्ट जैव-संगतता के लिए उपयोग किया जाता है। पारंपरिक रूप से, NDs का संश्लेषण ऊर्जा-गहन तरीकों से किया जाता है, जिसमें खतरनाक रसायनों की आवश्यकता होती है और प्रतिक्रिया समय लंबा होता है। अधिक टिकाऊ विकल्पों की आवश्यकता को पहचानते हुए, इस अध्ययन में सामान्य तापमान और दबाव पर प्रोब अल्ट्रासोनिकेशन द्वारा NDs के संश्लेषण की जांच की गई है, जिसमें जलीय माध्यम में कार्बनिक लवणों का प्रीकर्सर के रूप में उपयोग किया गया है। यह विधि पर्यावरणीय प्रभाव और संचालन की जटिलता को काफी कम कर देती है। FESEM, HRTEM, FTIR, Raman और XRD जैसी विशेषता तकनीकों से पता चला कि अल्ट्रासोनिकेशन समय एक महत्वपूर्ण कारक है: कम समय (30 मिनट) पर मेटास्टेबल संरचनाएँ बनती हैं, जबकि लंबे अल्ट्रासोनिकेशन (1 घंटा) पर उच्च गुणवत्ता वाले क्यूबिक नैनोडायमंड बनते हैं। अम्ल शुद्धिकरण डायमंड रमन पीक को  $1332\text{ cm}^{-1}$  पर और अधिक स्पष्ट करता है और क्यूबिक क्रिस्टल संरचना की पुष्टि करता है, जिससे यह सिद्ध होता है कि यह हरित विधि अच्छी तरह से परिभाषित NDs का विश्वसनीय उत्पादन कर सकती है और PET सतह पर इन-सीटू और एक्स-सीटू अनुप्रयोग के माध्यम से जल-अवशोषण और अग्नि प्रतिरोध जैसे बहु-कार्यात्मक गुण प्राप्त किए जा सकते हैं। यह विकास उन्नत

वस्त्र अनुप्रयोगों के लिए नैनोडायमंड के बड़े पैमाने पर उत्पादन को सक्षम बनाता है, वह भी पर्यावरण सुरक्षा से समझौता किए बिना।

NDs के हरित संश्लेषण के आधार पर, अध्ययन का अगला भाग PET वस्त्रों पर उनकी प्रत्यक्ष अनुप्रयोग की चर्चा करता है, ताकि PET कपड़े की ज्वलनशीलता और जल-विरोधिता की समस्या को हल किया जा सके। इस अध्ययन में एक नवीन इन-सीटू दृष्टिकोण अपनाया गया है, जिसमें कार्बन नैनोस्ट्रक्चर को वायुमंडलीय दबाव डाइइलेक्ट्रिक प्लाज्मा का उपयोग कर सीधे PET सतह पर संश्लेषित किया गया। इस दृष्टिकोण से स्वतंत्र रूप से नैनोपार्टिकल संश्लेषण और बाद में जमा करने की आवश्यकता समाप्त हो जाती है, जिससे वस्त्र रेशों पर नैनोडायमंड कोटिंग अधिक स्थायी और एकसमान रूप से जुड़ जाती है। FESEM और HRTEM विश्लेषण कार्बन नैनोस्ट्रक्चर की उपस्थिति और संरचना की पुष्टि करते हैं, जबकि Raman और FTIR स्पेक्ट्रोस्कोपी NDs के निर्माण और कपड़े के साथ उनके रासायनिक एकीकरण को प्रमाणित करते हैं। कार्यात्मक PET वस्त्रों में लौ प्रतिरोधकता में उल्लेखनीय सुधार देखा गया, जिसमें LOI मान 26-28 तक पहुंचे, साथ ही हाइड्रोफिलिसिटी में भी वृद्धि हुई, जो सक्रिय परिधान में आराम और नमी प्रबंधन के लिए महत्वपूर्ण है। इन-सीटू फंक्शनलाइजेशन प्रक्रिया को सरल बनाता है और वस्त्रों में स्थायी, बहु-कार्यात्मक गुण प्रदान करता है।

जहाँ NDs के उपचार से लौ प्रतिरोध और सतह की हाइड्रोफिलिसिटी में उल्लेखनीय सुधार हुआ, वहीं उच्च-प्रदर्शन सक्रिय परिधान के लिए नमी प्रबंधन और UV सुरक्षा में और सुधार की आवश्यकता थी। इसी उद्देश्य से, हाइड्रॉक्सीएपेटाइट (HAp), जो हड्डी और दांत में पाया जाने वाला एक जैव-संगत सिरेमिक है, को PET वस्त्रों के लिए सतह कोटिंग के रूप में आजमाया गया। इस अध्ययन में, HAp को दो अलग-अलग रासायनिक प्रीसिपिटेशन विधियों (HAp1 और HAp2) द्वारा संश्लेषित किया गया और डिप-पैड-क्योर प्रक्रिया द्वारा PET पर एक्स-सीटू लगाया गया। दोनों HAp कोटिंग्स ने जल-अवशोषण, विकिरण क्षमता, त्वरित-सुखाने के व्यवहार और अल्ट्रावायलेट सुरक्षा कारक (UPF) में उल्लेखनीय सुधार दिखाया। हालांकि, HAp1 से उपचारित वस्त्रों ने बेहतर प्रदर्शन और स्थायित्व दिखाया, यहाँ तक कि कई धोने के

बाद भी। FESEM, FTIR, Raman और XPS द्वारा किए गए विस्तृत विश्लेषण से पता चला कि HAp1 प्रक्रिया से सूक्ष्म कण बनते हैं, जो PET फाइबर सतह के साथ अधिक घनिष्ठ रूप से संपर्क करते हैं, जिससे मजबूत चिपकाव और अधिक मजबूत कार्यात्मक गुण मिलते हैं। HAp कोटिंग्स का सफल अनुप्रयोग न केवल PET की जल-विरोधिता को दूर करता है, बल्कि बहु-कार्यात्मकता भी प्रदान करता है।

HAp कोटिंग्स के आशाजनक परिणामों को देखते हुए, आगे के अध्ययन PET वस्त्रों पर सीधे हाइड्रॉक्सीएपेटाइट (In-HAp1 और In-HAp2) के इन-सीटू संश्लेषण की ओर निर्देशित किए गए। इस दृष्टिकोण का उद्देश्य HAp के कार्यात्मक लाभों को अधिकतम करना और वास्तविक परिस्थितियों में दीर्घकालिक स्थायित्व सुनिश्चित करना था। इन-सीटू डिप-पैड-क्योर विधि ने एक समान और सतत HAp परत बनाई, जिसमें विशेष रूप से In-HAp1 ने नैनोस्केल कोटिंग दी, जो फाइबर सतह से मजबूती से जुड़ी रही। FESEM, FTIR, Raman और XPS द्वारा किए गए व्यापक मूल्यांकन से पता चला कि In-HAp1-उपचारित वस्त्रों ने अपनी बेहतर UPF और नमी प्रबंधन की विशेषताएँ बार-बार धोने के बाद भी बनाए रखीं, और In-HAp2 से बेहतर प्रदर्शन किया। इस बेहतर प्रदर्शन का श्रेय In-HAp1 प्रक्रिया में नियंत्रित वृद्धि और सूक्ष्म कण आकार को जाता है, जिससे PET सब्सट्रेट के साथ मजबूत संपर्क स्थापित होता है, जो पहले के एक्स-सीटू HAp कोटिंग से भी अधिक था। HAp के हाइड्रोफिलिक और UV-ब्लॉकिंग गुणों का लाभ उठाकर, यह अनुकूलित सतह संशोधन PET को एक सच्चा बहु-कार्यात्मक वस्त्र बना देता है, जो टिकाऊ, उच्च-प्रदर्शन सक्रिय परिधान के लिए आदर्श है।

इस शोध का प्रत्येक भाग पिछले हिस्से पर आधारित है, जो नैनोडायमंड संश्लेषण की टिकाऊ विधि के विकास से शुरू होकर, उनके प्रत्यक्ष अनुप्रयोग द्वारा PET में लौ प्रतिरोध और हाइड्रोफिलिसिटी लाने, और फिर जैव-सिरेमिक जैसे हाइड्रॉक्सीएपेटाइट कोटिंग्स द्वारा नमी प्रबंधन और UV सुरक्षा में और सुधार करने तक जाता है। इन उन्नत सतह संशोधनों को एकीकृत करके, यह शोध स्मार्ट, बहु-कार्यात्मक और टिकाऊ वस्त्रों की अगली पीढ़ी के लिए एक आधार तैयार करता है।



# TABLE OF CONTENTS

<b>CONTENTS</b>	<b>Page</b>
	<b>No.</b>
Certificate	i
Acknowledgments	iii
Abstract	vii
Table of contents	xv
Lists of Figures	xxi
List of Tables	xxxix
List of Symbols and Abbreviations	xxxviii
<b>Chapter 1: Introduction and Literature Review</b>	<b>1</b>
1.1 Introduction	3
1.2 Enhancing PET textile properties through surface modification	4
1.3 Overview of different methods for PET surface modification	5
1.4 Surface modifications for other potential multifunctional applications	7
1.5 Literature review of surface modification	9
1.5.1 Chemical surface modification	9
1.5.2 Grafting techniques	13
1.5.3 Plasma-based surface modification	15

1.5.4	Application of nanomaterials for PET surface functionalization	18
a	Metal and metal oxide nanoparticles for enhanced functionality	19
b	Carbon-based nanomaterials	23
c	Polymer nanoparticles and their limitations	26
1.6	Nanodiamonds as an emerging material for surface modification of textiles	28
1.7	Hydroxyapatite, a bioceramic for functionalization of textiles	32
1.8	Research gaps and motivations	37
1.9	Aim and objectives	39
1.10	Thesis organization	40
 <b>Chapter 2: Ultrasonication-Mediated Nanodiamond Synthesis and its Application on PET Fabric</b>		 43
2.1	Introduction	45
2.2	Materials and methods	46
2.2.1	Materials	46
2.2.2	Synthesis of USND by ultrasonication	46
2.2.3	Application on PET fabric	47
2.2.4	Wash durability	48
2.2.5	Characterization	48
a	Morphological and chemical	48
b	Functional properties of the treated fabric	49

2.3	Results and Discussion	50
2.3.1	Morphology of carbon nanostructures	51
2.3.2	HRTEM analysis	59
2.3.3	Chemical analysis of nanodiamonds	66
2.3.4	Treated Fabric Performance evaluation	85
	a Hydrophilicity of treated PET	85
	b Flammability test of treated PET	86
 <b>Chapter 3: Atmospheric Pressure Plasma-Mediated <i>In-situ</i> Synthesis of Nanodiamonds on PET Fabrics</b>		<b>89</b>
3.1	Introduction	91
3.2	Materials and methods	91
	3.2.1 Materials	91
	3.2.2 Synthesis of nanodiamonds by plasma	92
	3.2.3 <i>In-situ</i> synthesis of nanodiamonds on PET fabric surfaces	93
	3.2.4 Wash durability	93
	3.2.5 Characterizations	94
3.3	Results and discussion	95
	3.3.1 Morphologies of NDs and treated PET	98
	3.3.2 HRTEM synthesized carbon nanostructures	105
	i Using Ethanol/Argon (Eth/Ar) plasma	105
	ii Using Ethanol/Nitrogen (Eth/N <sub>2</sub> ) plasma	109
	3.3.3 Chemical analysis of <i>in-situ</i> synthesized carbon nanostructures	111
	3.3.4 Treated Fabric Performance evaluation	123

a	Hydrophilicity of treated PET	123
b	Flammability by LOI	128
c	Physical appearance and mechanical properties	130

## **Chapter 4: Synthesis and Characterisation of Hydroxyapatite and its *Ex-* 135**

### ***situ* Application on PET Fabric**

4.1	Introduction	137
4.2	Materials and methods	138
4.2.1	Materials	138
4.2.2	Preparations of HAp1	138
4.2.3	Preparations of HAp2	138
4.2.4	Application of as-prepared HAp1 and HAp2 suspensions on PET Fabric	139
4.2.5	Wash durability	139
4.2.6	Characterization	142
4.3	Results and Discussion	143
4.3.1	Morphology of HAp and HAp treated PET	145
4.3.2	Chemical analysis	149
4.3.3	Treated fabric performance evaluation	168
a	Hydrophilicity of treated PET	168
b	Ultraviolet protection factor	171
c	IR thermal micrographs	175
d	Physical properties	177

## Chapter 5: *In-situ* Synthesis and Application of Hydroxyapatite on the PET 181

### Fabric

5.1	Introduction	183
5.2	Materials and methods	184
5.2.1	Materials	184
5.2.2	Application of hydroxyapatite on PET fabric by <i>in-situ</i> synthesis	184
5.2.3	Synthesis of hydroxyapatite particles for comparison	185
5.2.4	Wash durability	185
5.2.5	Characterizations	185
5.3	Results and Discussion	186
5.3.1	Morphology of <i>in-situ</i> HAp treated PET	187
5.3.2	Chemical analysis	191
5.3.3	Treated Fabric Performance evaluation	207
a	Hydrophilicity of treated PET	207
b	Ultraviolet protection factors	211
c	IR thermal micrographs	214
d	Physical properties	215

<b>Chapter 6: Conclusions and Future Scope</b>	<b>221</b>
6.1 Conclusions	223
a Ultrasonication-mediated nanodiamond synthesis and its application on PET Fabric	224
b Atmospheric pressure plasma mediated <i>in-situ</i> synthesis of nanodiamonds on PET Fabrics	225
c Synthesis and characterization of hydroxyapatite and its <i>ex-situ</i> application on PET fabric	226
d <i>In-Situ</i> synthesis and application of hydroxyapatite on the PET Fabric	227
6.2 Future Scope	228

## LIST OF FIGURES

<b>Figure No.</b>	<b>Caption of the figure</b>	<b>Page No.</b>
Figure 2.1	Photographs of (a) Reaction mixture; Reaction mass at different ultrasonication times (b) 10 min, (c) 30 min, (d) 1 h and (e) 2 h	51
Figure 2.2	Growth morphology of (a) Growth of carbon-nanostructures observed in reaction time of 10 min of ultrasonication, (b) schematic representation of the growth of pyramid-shaped carbon nanostructures	52
Figure 2.3	Schematic representation of the growth of pyramid-shaped carbon nanostructures and its reaction during nucleation to form nanodiamonds	53
Figure 2.4	FESEM images of (a) 10US/ND, (b) 30US/ND, (c) 60US/ND (inset: size distribution of particles having an average size of 0.340 $\mu\text{m}$ ), (d) 120US/ND	55
Figure 2.5	FESEM images of acid purified 60US/ND at different magnifications	56
Figure 2.6	FESEM images of (a,b) Control PET, (c,d) Ex/60USND/PET and (e,f) In/60USND/PET	57
Figure 2.7	HRTEM images and SAED patterns of (a,b) 10US/ND and (c,d) 30US/ND	59

Figure 2.8	HRTEM images and SAED patterns of (a,b) 60US/ND and (c,d) 120US/ND.	60
Figure 2.9	HRTEM image (b) fringes showing d-spacing (c) SEAD pattern of acid purified 60US/ND particle.	63
Figure 2.10	(a,b) HRTEM image (c,d) fringes showing d-spacing (e,f) SEAD pattern of few more acid purified 60US/ND particle	65
Figure 2.11	Full FTIR spectra of different US/NDs from 500 to 4000 $\text{cm}^{-1}$	67
Figure 2.12	FTIR spectra of different US/NDs in (a) 750 to 2000 $\text{cm}^{-1}$ (b) 2750 to 4000 $\text{cm}^{-1}$ .	68
Figure 2.13	FTIR spectra of as-prepared and acid-purified 60US/NDs	70
Figure 2.14	FTIR spectra of Control PET, Ex/60USND/PET and In/60USND/PET (a) 500-1800 $\text{cm}^{-1}$ (b) 1300 to 1500 $\text{cm}^{-1}$	71
Figure 2.15	Raman spectra of US/NDs synthesized for different reaction times	73
Figure 2.16	Raman spectra of the 60US/ND sample purified in acid mixture for 60 min (a) focused (bright spot) and (b) unfocused (dark spot)	75
Figure 2.17	Raman mapping of acid-purified (for 1.5 h) 60US/ND sample at 1332 $\text{cm}^{-1}$ with Raman spectra (a) focused (bright spot) and (b) unfocused (black/dark spot)	76
Figure 2.18	Raman spectra of Control PET, Ex/USND/PET and In/USND/PET	78

Figure 2.19	XRD patterns of 60US/ND acid purified nanodiamond	79
Figure 2.20	DLS study (a and b) size distribution by number and intensity and Zeta potential distribution	81
Figure 2.21	Flammability test of 5 cm PET fabrics: Comparison of Control, Ex/60USND/PET, and In/60USND/PET before and after 10 washing cycles	87
Figure 3.1	I-V curves of atmospheric plasma with ethanol vapors in (a) argon and (b) nitrogen	96
Figure 3.2	Photographs of the plasma glow obtained using (a) Eth/Ar and (b) Eth/N <sub>2</sub>	96
Figure 3.3	Schematic of the <i>in-situ</i> synthesis of nanodiamonds on PET fabric surface	97
Figure 3.4	FESEM images at different magnifications of carbon nanostructures formed using ethanol/argon plasma (Eth/Ar-ND).	99
Figure 3.5	FESEM image at different magnifications of carbon nanostructures formed using ethanol/nitrogen plasma (Eth/N <sub>2</sub> -ND).	100
Figure 3.6	FESEM images of PET fabrics: (a,b) control at different magnifications	102
Figure 3.7	FESEM images of PET fabrics: (a,b) treated with argon plasma (Ar/PET) at different magnifications.	102
Figure 3.8	FESEM images of PET fabrics: (a,b) treated with nitrogen plasma (N <sub>2</sub> /PET) at different magnifications	103

Figure 3.9	FESEM images of PET fabrics: (a,b) treated with ethanol/argon plasma (Eth/Ar-PET) at different magnifications	103
Figure 3.10	FESEM images of PET fabrics: (a,b) treated with ethanol/nitrogen plasma (Eth/N <sub>2</sub> -PET) at different magnifications	104
Figure 3.11	HRTEM image of nanodiamond synthesized in ethanol/argon plasma (Eth/Ar-ND) (a, b) crystalline particles, (c) SAED pattern of crystalline particles	106
Figure 3.12	HRTEM image of nanodiamond synthesized in ethanol/argon plasma (Eth/Ar-ND) (a, b) single crystal carbon structure (c) SAED pattern showing plane [111] of a high quality crystal.	107
Figure 3.13	HRTEM image of ethanol/nitrogen plasma (Eth/N <sub>2</sub> -ND) synthesized nanodiamonds (a) nanoparticles, (b) lattice fringes of nanoparticles, and (c) SAED pattern	109
Figure 3.14	HRTEM images (a) and SAED patterns (b) of particles obtained after digestion of Eth/Ar plasma-treated PET fabric	110
Figure 3.15	HRTEM images (a) and SAED patterns (b) of particles obtained after digestion of Eth/N <sub>2</sub> plasma-treated PET fabric	110
Figure 3.16	FTIR spectra of (a) synthesized nanodiamonds collected from plasma exhaust and (b) nanodiamonds isolated from the plasma-treated PET fabrics	112

Figure 3.17	ATR-FTIR spectra of control-PET, Ar-plasma PET (Ar/PET), and ethanol/Ar plasma (Eth/Ar-PET)-treated PET fabrics in two selected regions	113
Figure 3.18	ATR-FTIR spectra of control-PET, N <sub>2</sub> -plasma treated PET (N <sub>2</sub> /PET), and ethanol/N <sub>2</sub> plasma-treated PET fabric (Eth/N <sub>2</sub> -PET) in two selected regions.	115
Figure 3.19	Raman spectra of unpurified Eth/Ar and Eth/N <sub>2</sub> plasma synthesized nanodiamonds collected from the exhaust of the plasma reactor	117
Figure 3.20	Raman spectra of Eth/Ar, Eth/N <sub>2</sub> plasma synthesized nanodiamonds collected from the exhaust of the plasma reactor and purified by acid treatment	117
Figure 3.21	Raman spectra of plasma treated samples compared to the control PET using (a) Ar (b) N <sub>2</sub> plasma	120
Figure 3.22	Deconvoluted Raman spectra of nanodiamonds (NDs) particles obtained after digestion of (a) Eth/Ar plasma-PET and (b) Eth/N <sub>2</sub> plasma-PET fabrics	121
Figure 3.23	Images of the drops (standard AATCC-79) which are not absorbed in (a and b) Control PET and contact angle of drop is more than >130° and are absorbed instantly in treated (c) (Ar/PET), (d) (Eth/Ar-PET), (e) (N <sub>2</sub> /PET) and (f) (Eth/N <sub>2</sub> -PET)	124
Figure 3.24	Water Drop Spreading profile obtained from Moisture Management Test (MMT) (a) Control PET, (b)Ar/PET, (c) Eth/Ar-PET, (d) N <sub>2</sub> /PET and (e) Eth/N <sub>2</sub> -PET	125
Figure 3.25	(a) Photographic images, (b) whiteness indices of the control and treated PET fabrics.	131

Figure 3.26	Tensile properties (a) mechanical strength (expressed as load), and (b) % elongation at break of the control and treated PET fabrics	132
Figure 4.1	Schematic illustration of hydroxyapatite (HAp1) synthesis reaction and dispersion preparation using $H_3PO_4$ and $Ca(OH)_2$ solutions	140
Figure 4.2	Schematic illustration of hydroxyapatite (HAp2) synthesis reaction and dispersion preparation using $Na_2HPO_4$ and $CaCl_2$ solutions	141
Figure 4.3	Schematic of PET fabric surface modification process	144
Figure 4.4	FESEM images of (a and b) HAp1 powders at two different magnifications	144
Figure 4.5	FESEM images of (a and b) HAp2 powders at two different magnifications	145
Figure 4.6	FESEM Images of (a and b) Control PET, (c and d) PET/HAp1 and (e and f) PET/HAp2	146
Figure 4.7	FESEM images of (a and b) 10 wash and (c and d) 30 wash of PET/HAp1	147
Figure 4.8	FESEM images of (a and b) 10 wash and (c and d) 30 wash of PET/HAp2	149
Figure 4.9	EDX mapping of (a-d and i) HAp1 and (e-h and j) HAp2	150
Figure 4.10	EDX Elemental Mapping of (a,d,g) Control PET, (b,e,h,j,l) PET/HAp1 and (c,f,i,k,m) PET/HAp2	151

	Fabrics: (a–c) FESEM Images; (d–f) Carbon Mapping; (g–i) Oxygen Mapping; (j, k) Phosphorus Mapping; (l, m) Calcium Mapping	
Figure 4.11	FTIR-ATR spectra of (a) HAp1 and (b) HAp2 full spectra	154
Figure 4.12	FTIR-ATR spectra of (a) control PET and PET/HAp1 and (b) control PET and PET/HAp2 (Wavelength range 500-2000 $\text{cm}^{-1}$ )	155
Figure 4.13	FTIR-ATR spectra of (a) control PET and PET/HAp1 and (b) control PET and PET/HAp2 (Wavelength range 2000-4000 $\text{cm}^{-1}$ )	156
Figure 4.14	Raman spectra of (a) HAp1, PET-HAp1 and Control PET, (b) deconvoluted spectra of PET-HAp1 in selected range	158
Figure 4.15	Raman spectra of (a) HAp2, PET-HAp2 and Control PET, (b) deconvoluted spectra of PET-HAp2 in selected range	159
Figure 4.16	Full XPS spectra of HAp1, HAp2, Control PET, PET/HAp1 and PET/HAp2	162
Figure 4.17	XPS spectra of (a and d) control PET, (b,e,g and i) HAp1, (c,f,h and j) HAp2	136
Figure 4.18	XPS spectra of (a,c,e and g) PET/HAp1 and (b,d,c and h) PET/HAp2	164
Figure 4.19	Schematic illustration of the hydroxyapatite interactions with PET fabric	167

Figure 4.20	Hydrophilicity performance (a) Water drop absorbency times (DAT), (b) water wicking heights of fabrics before and after washings	169
Figure 4.21	Ultraviolet protection factors (UPF) value of fabrics before and after washing	171
Figure 4.22	Infra-Red camera micrographs of wetted untreated and treated PET fabric samples with time on a surface maintained at 37 °C	173
Figure 4.23	Plot of water spreading area Vs time and % evaporation of untreated and treated PET fabric samples derived from Figure 4.20	174
Figure 4.24	Physical strength (a) Breaking load, (b) Tearing force of control-PET, PET/HAp1 and PET/HAp2 fabrics	177
Figure 4.25	Bar graph of (a) Bending length and (b) Whiteness index of control-PET, PET/HAp1 and PET/HAp2 fabrics	178
Figure 5.1	Schematic illustration of the <i>in-situ</i> surface modification steps	186
Figure 5.2	FESEM Images of (a and b) Control PET, (c and d) PET/In-HAp1 and (e and f) PET/In-HAp2	188
Figure 5.3	FESEM Images of (a and b) 10 wash and (c and d) 30 wash PET/In-HAp1	189
Figure 5.4	FESEM Images of (a and b) 10 wash and (c and d) 30 wash PET/In-HAp2	190

Figure 5.5	EDX Elemental Mapping of (a,d,g) Control PET, (b,e,h,j,l) PET/In-HAp1 and (c,f,i,k,m) PET/In-HAp2 Fabrics: (a–c) FESEM Images; (d–f) Carbon Mapping; (g–i) Oxygen Mapping; (j, k) Phosphorus Mapping; (l, m) Calcium Mapping	192
Figure 5.6	FTIR-ATR spectra of treated samples in comparison to control PET (Wavelength range 500-2000 $\text{cm}^{-1}$ )	193
Figure 5.7	FTIR-ATR spectra of treated samples in comparison to control PET (Wavelength range 2000-4000 $\text{cm}^{-1}$ )	194
Figure 5.8	Raman spectra of (a)PET/In-HAp1 and Control PET, (b) Deconvoluted Raman Spectra of PET/In-HAp1	197
Figure 5.9	Raman spectra of (a) HAp2, PET/In-HAp2 and Control PET; (b) Deconvoluted Raman Spectra of PET/In-HAp2	198
Figure 5.10	Full XPS spectra of control PET, HAp1, HAp2, PET/HAp1 and PET/HAp2 sample	202
Figure 5.11	XPS spectra of (a,c,e and g) PET/In-HAp1 and (b,d,f and h) PET/In-HAp2.	204
Figure 5.12	Hydrophilicity test (a) Water drop absorbency times (DAT), (b) water wicking heights of fabrics before and after washings.	208

Figure 5.13	Ultraviolet protection factors (UPF) value of fabrics before and after washings	209
Figure 5.14	Infra-Red camera micrographs of wetted untreated and treated PET fabric samples with time on a surface maintained at 37 °C	212
Figure 5.15	Plot of water spreading area Vs time and % evaporation of untreated and treated PET fabric samples derived from Figure 5.12	213
Figure 5.16	Physical strength (a) Breaking load , (b) Tearing force of control PET, PET/In-HAp1 and PET/In-HAp2 fabrics	216
Figure 5.17	Bar graph of (a) Bending length and (b) Whiteness index of control PET, PET/In-HAp1 and PET/In-HAp2 fabric	217

## LIST OF TABLES

<b>Table no.</b>	<b>Title of table</b>	<b>Page no.</b>
Table 1.1	Application of nanomaterials for surface modification of textiles	25
Table 2.1	<i>d</i> -Spacings and estimated <i>hkl</i> values obtained from SAED patterns of different US/NDs in comparison to the reported literatures values	62
Table 2.2	Comparison of nanodiamonds synthesized by different methods	82
Table 2.3	Effect of washing cycles on water drop absorbency time of the control and treated fabrics	85
Table 3.1	Comparison of experimental versus theoretical values of <i>d-spacing</i> of cubic nanodiamond structures corresponding to different <i>hkl</i> planes ( $d_{\text{exp}}$ : experimental <i>d-spacing</i> and, $d_{\text{theo}}$ : <i>d-spacing</i> reported in the cited literature).	108
Table 3.2	Effect of ageing time on water drop absorbency time of the control and treated fabrics	127
Table 3.3	Effect of washing cycles on water drop absorbency time of the control and treated fabrics	127
Table 3.4	Limiting oxygen index values of the control and treated fabrics	129

Table 4.1	Binding energy (eV) of elements present in the XPS spectra of control PET, HAp1, HAp2, PET/HAp1 and PET/HAp2 samples	165
Table 5.1	Binding energy (eV) of elements present in the XPS spectra of control PET, HAp1, HAp2, PET/In-HAp1 and PET/In-HAp2 samples	205
Table 5.2	Comprehensive performance evaluation and comparison of <i>in-situ</i> and <i>ex-situ</i> treated PET fabric	219

## LIST OF SYMBOLS/ABBREVIATIONS

<b>Symbols/Abbreviations</b>	<b>Expanded form/Term</b>
<i>PET</i>	Poly(ethylene terephthalate)
V	Voltage
I	Current
<i>nm</i>	nanometer
<i>h</i>	hour
<i>NDs</i>	Nanodiamonds
<i>USND</i>	Ultrasonication synthesized nanodiamonds
<i>FE-SEM</i>	Field emission scanning electron microscopy
<i>EDX</i>	Energy-dispersive X-ray spectroscopy
<i>HR-TEM</i>	High resolution transmission electron microscope
<i>FTIR</i>	Fourier transform infrared spectroscopy
<i>XPS</i>	X-ray photoelectron spectroscopy
$\text{Å}$	Angstrom
<i>hkl</i>	Crystallographic planes
<i>SAED</i>	Selected area electron diffraction
<i>HAp</i>	Hydroxyapatite
<i>In-HAp</i>	<i>In-situ</i> synthesized hydroxyapatite
<i>M</i>	Molarity
<i>IR Micrograph</i>	Infra red camera images
<i>DAT</i>	Drop absorption time

<i>Ar</i>	Argon
<i>N<sub>2</sub></i>	Nitrogen
<i>Eth</i>	Ethanol
<i>UPF</i>	Ultra-Violet Protection Factor